JOURNAL OF CATALYSIS 106, 369–377 (1987)

CO Chemisorption over MnO_x-Modified Ni(111): Importance of Perimeter Sites in Strong Metal–Support Interaction

YONG-BO ZHAO AND YIP-WAH CHUNG

Department of Materials Science and Engineering, Northwestern University, Evanston, Illinois 60201

Received November 6, 1986; revised March 10, 1987

CO chemisorption on both clean Ni(111) and MnO_x (x is between 0.2 and 0.5)-modified Ni(111) surfaces at 200°K have been studied by Auger electron spectroscopy (AES), thermal desorption spectroscopy (TDS), and high-resolution electron energy loss spectroscopy (HREELS). The MnO_x/Ni specimen was prepared by evaporating MnO_2 powder to the Ni surface and then reducing the specimen at 700°K. TDS results showed that the presence of surface MnO_x species suppresses CO chemisorption and that the suppression is almost a linear function of the MnO_x coverage. The most prominent CO desorption peak on Ni occurs at 415°K. This peak intensity decreased with increasing MnO_x coverage, indicating a site-blocking effect. An additional CO desorption peak at 305°K was found on the MnO_x-modified Ni surface. This 305°K peak intensity attains a maximum at some intermediate MnO_x coverage. HREELS showed a new C–O stretching frequency of 1620 cm^{-1} for CO adsorbed on the MnO_x/Ni surface. The disappearance of this 1620-cm^{-1} energy loss peak upon heating the surface to 325°K suggests that both the 305°K TDS peak and the 1620-cm^{-1} energy loss peak represent the same adsorbed CO state, which is attributed to CO adsorbed on MnO_x/Ni perimeter sites. Surface morphology of the oxide islands and significance of the perimeter sites are discussed along with experimental results. © 1987 Academic Press, Inc.

INTRODUCTION

The nature of strong metal–support interaction (SMSI) between Group VIII metals and certain oxides such as titania and lanthana has received considerable attention since Tauster and co-workers reported their pioneering work on the subject (*1, 2*). It is generally accepted that under the typical conditions required to induce SMSI (reduction in H_2 at 773°K), the support oxide migrates to the metal surface in a reduced state (*3–15*) and acts either as a promoter or poison. The catalytic properties of such a system can be changed dramatically. Some of the most pronounced effects are the suppression of CO and H_2 chemisorption and enhancement of the CO hydrogenation activity (*1, 2, 7, 8, 11–23*).

Given that the metal surface is partially covered by a reduced oxide, one is confronted with the problem of explaining both chemisorption suppression and enhancement of CO hydrogenation activity (*24–26*). When a metal catalyst is in the SMSI state as defined above, the metal surface consists of three types of sites: clean metal atoms, reduced oxide surface, and perimeter sites between the two. Since the oxide is usually inactive, surface metal sites covered by the oxide will not be able to participate in chemisorption and catalytic reactions. Although it was found that the chemisorption suppression is due to either simple physical blocking by the surface oxide species (*21*) or physical blocking plus electronic interaction (*13–15*), the extent of such a suppression and activity loss is basically determined by the actual physical coverage of the oxide. On the other hand, the perimeter of the oxide islands on top of the metal provides a unique ensemble of sites that may possess a higher CO hydrogenation activity to offset the activity loss due to physical blocking by the surface oxide. This enhancement of CO hydrogenation activity can be due to more effective competition of H_2 versus CO che-

0021-9517/87 $3.00
Copyright © 1987 by Academic Press, Inc.
All rights of reproduction in any form reserved.

misorption (*19, 25*) or faster CO dissociation (*26*).

In a previous study of the Ni/MnO_x system, it was found that MnO_x migrates to the metal surface rapidly at temperatures as low as 500°K (*10*). In another study of CO chemisorption on a Mn-promoted Rh/SiO_2 catalyst, a low C–O stretching frequency at 1520 cm^{-1} was observed (*27*). Taken together, these observations suggest that a MnO_x-modified Ni surface could be an interesting SMSI system for further investigation.

The present study was conducted to investigate effects of MnO_x surface species on CO chemisorption on Ni(111) and to establish a correlation between CO chemisorption and surface morphology of the oxide. In particular, experiments were carried out to characterize the surface composition, stretching frequency of adsorbed CO, and the amount of CO adsorbed on the surface under different conditions.

EXPERIMENTAL

All experiments were carried out in an ultrahigh vacuum (UHV) chamber which was equipped with an Auger electron spectrometer, a metal/oxide evaporator, an ion gun, a quadrupole mass spectrometer, and a high-resolution electron energy loss spectrometer. A schematic diagram of this setup is shown in Fig. 1. The specimen was mounted on a manipulator that could be moved to different positions for surface preparation and data acquisition. The specimen could be cooled to 200°K, or heated at up to 7°K/s to 800°K. The surface temperature was monitored with a W/5% Re–W/26% Re thermocouple spot-welded to the specimen surface.

The specimen used in these experiments was a Ni(111) single crystal disk about 1 cm^2 in surface area and 1 mm in thickness. The surface was cleaned by Ar ion sputtering and annealing at 700°K under UHV for a few cycles. The evaporation source was MnO_2 powder that was held in a Ta boat. During evaporation, the boat was heated to about 800°K with the Ni crystal held at room temperature. Auger electron spectroscopy (AES) showed that such a procedure resulted in a surface oxide with an oxygen-to-manganese atomic ratio close to

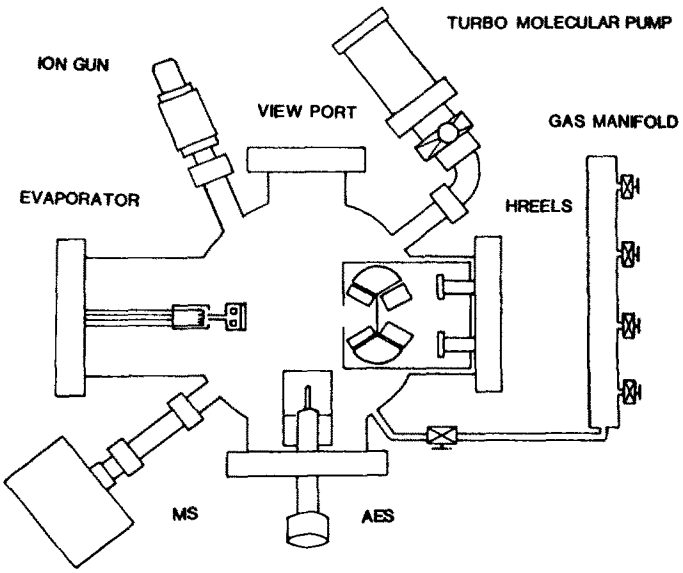

FIG. 1. Schematic diagram of the experimental setup. MS, mass spectrometer; AES, Auger electron spectrometer; HREELS, high-resolution electron energy loss spectrometer.

one. The oxygen-to-manganese ratio was calibrated using Mn and MnO_2 standard samples. The surface was then reduced at 700°K under UHV or H_2 for about 10 min. From our experience, such a reduction treatment will produce an unoxidized and smooth nickel surface. The final oxygen-to-manganese ratio was between 0.2 and 0.5. AES was used to verify that the surface was clean after each step of preparation. After a surface was prepared, it was cooled to 200°K for CO exposure. Carbon monoxide (99.99% purity) was purified by passing it through a liquid-nitrogen-cooled stainless-steel thin tubing to remove residual water and metal carbonyls before it was introduced into the chamber. In all experiments, the CO exposure was fixed at 30 Langmuirs (L). AES was performed at a primary electron energy of 1600 eV using a Comstock electron analyzer at a pass energy of 50 eV and a modulation amplitude of 2 eV. The surface composition was characterized by four major Auger peaks at 272 eV (C), 503 eV (O), 589 eV (Mn), and 848 eV (Ni). Thermal desorption was performed by ramping the temperature of the Ni specimen from 200 to 700°K at 7°K/s. In high-resolution electron energy loss spectroscopy (HREELS) studies, the electron beam was set at 2 eV primary energy (uncorrected for work function differences), and the surface was maintained at 200°K unless indicated otherwise. All energy loss spectra were taken with elastic peak resolution better than 80 cm^{-1}. The surface was cleaned and reprepared between thermal desorption or HREELS experiments.

RESULTS AND DISCUSSIONS

Several Ni(111) surfaces were prepared with different surface concentrations of MnO_x. The manganese-to-nickel Auger ratio ranged from 0 to 0.3, the latter value corresponding to an average oxide coverage about 1.3 monolayers according to Auger calibration. Results of CO thermal desorption from these surfaces are shown in Fig. 2. From a clean Ni(111) surface, the most prominent CO desorption peak is located at 415°K. With increasing amount of MnO_x on Ni, the 415°K peak becomes weaker. At the same time, a new feature at 305°K grows with increasing MnO_x coverage, reaches a maximum at an intermediate MnO_x coverage, and then decreases until it vanishes at a manganese-to-nickel Auger ratio of 0.3. Assuming validity of our calibration, the fact that the complete suppression of CO chemisorption occurred at an average oxide coverage of 1.3 instead of 1 monolayer indicates three-dimensional island formation for the oxide. In Fig. 3, areas under these two peaks are plotted as a function of the average surface MnO_x coverage (circles for 415°K TDS peak and

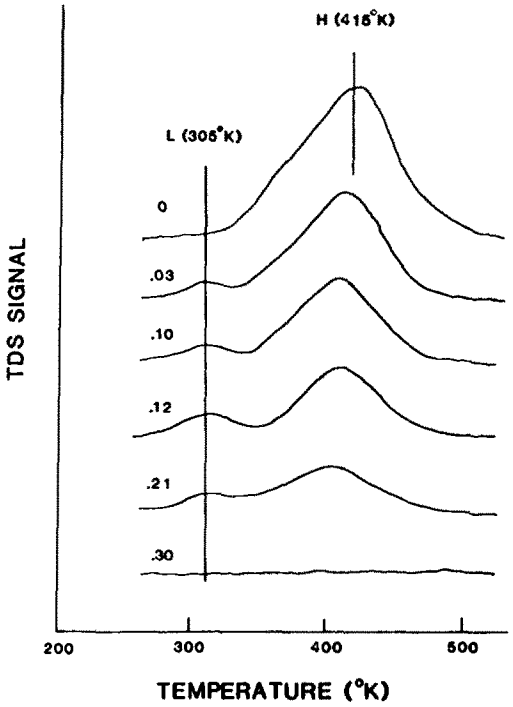

FIG. 2. Series of thermal desorption spectra of CO from the MnO_x-modified Ni(111) surface with different MnO_x coverages as indicated by the Auger Mn (589 eV)/Ni (848 eV) peak intensity ratio varying from 0 to 0.3. CO chemisorption was made by introducing 30 L CO into the UHV chamber while the specimen was at 200°K. During the thermal desorption process, the surface was heated at about 7°K/s.

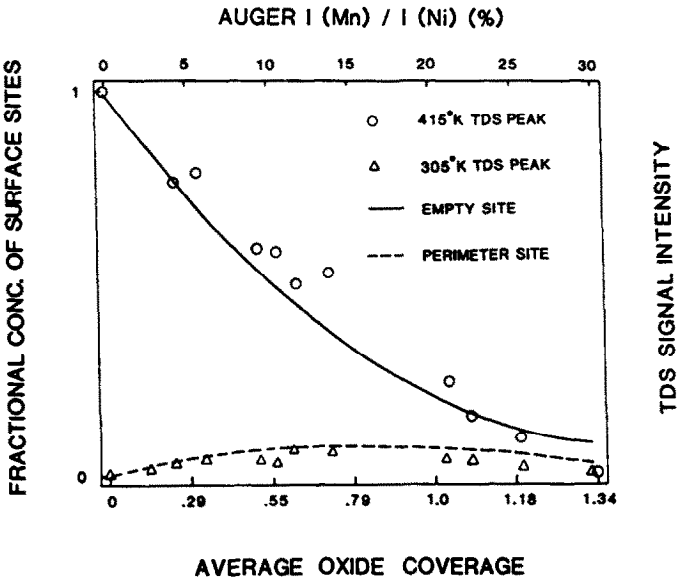

FIG. 3. Superimposed CO thermal desorption and Monte Carlo simulation results. For the TDS results, areas under both the 415°K TDS peak and the 305°K TDS peak are plotted as a function of average MnO_x coverage. The circles stand for the 415°K peak and the triangles for the 305°K peak. For the simulation results, fractional surface site concentration of a partially covered FCC (111) surface is plotted as a function of average oxide coverage. The oxide cluster size is fixed such that it blocks 169 surface sites. Oxide surface diffusion during reduction is simulated by allowing those adatoms beyond the first oxide layer to redisperse randomly three times onto the (111) surface with the same cluster size of 169 atoms. The solid curve stands for the uncovered sites and the broken one for perimeter sites. The top scale shows the Auger Mn (589 eV)/Ni (848 eV) peak intensity ratio (%). The bottom one gives the corresponding approximate average MnO_x coverage, as inferred from separate Auger calibration.

triangles for 305°K TDS peak). The 415°K peak decreases in intensity almost linearly with increasing MnO_x coverage. The fact that the 305°K peak attains a maximum at an intermediate oxide coverage can be interpreted readily in terms of CO adsorption at or near the perimeter of oxide islands on the Ni(111) surface. At low oxide coverage, the concentration of such perimeter sites is low. At sufficiently high oxide coverage, the nickel surface is completely covered, leading again to low perimeter site concentration. Therefore, at some optimum oxide coverage, the perimeter site concentration attains a maximum. Clearly, the optimum oxide coverage and the actual site concentration must depend on the average size of these oxide islands.

To illustrate this idea, we performed a simulation study with a face-centered-cubic (FCC) (111) surface representing the metal surface. For a given average oxide coverage, two-dimensional oxide patches (single layered clusters) with a size equivalent to n surface Ni sites (in the following discussion, we will call it as size n) are allowed to form randomly on the surface. As shown in Fig. 4, this results in the formation of three kinds of surface sites: empty (unblocked nickel) sites, covered (blocked Ni) sites, and perimeter sites. In each simulation, we fixed the value of n but allowed the oxide patches to overlap. Then all the adatoms beyond the first (oxide) layer were allowed to redisperse randomly onto the surface, to simulate oxide surface diffusion during reduction. At a given average oxide coverage, the concentration of these various surface sites (unblocked Ni sites, oxide sites, and perimeter sites) is a function of the

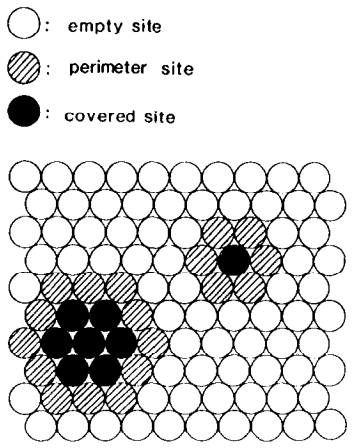

FIG. 4. Schematic diagram of a partially covered FCC (111) surface.

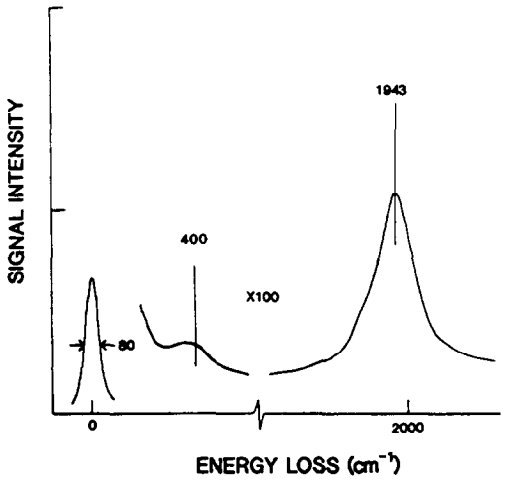

FIG. 5. High-resolution electron energy loss spectrum of 30 L CO adsorbed on clean Ni(111) surface at 200°K.

oxide cluster size n and the number of times r the overlapping oxide adatoms are allowed to redisperse. Assuming a one-to-one correspondence between the number of surface adsorption sites (clean Ni and perimeter sites) and the amount of CO desorbed (Fig. 3), we performed extensive calculations of the fraction of empty and perimeter sites at an average oxide coverage of one monolayer by varying n and r. A good match to the experimental data was obtained when $n = 169$ and $r = 3$ (*28*). Using the same two parameters, the concentration of empty and perimeter sites was calculated for all oxide coverages. Results of this calculation are superimposed onto the TDS data in Fig. 3 (solid curve for the empty site and broken curve for the perimeter site). Given the simplicity of the model and the simulation, the agreement between the experiment results and the simulation is quite remarkable.

Figure 5 shows the electron energy loss spectrum of CO adsorbed on a clean Ni(111) surface at 200°K. The major peaks at 400 cm^{-1} (carbon–metal stretching) and 1943 cm^{-1} (carbon–oxygen stretching due to bridge bonded CO on Ni) are well documented in the literature (*29–31*). Figure 6 shows the loss spectrum due to CO adsorbed on a Ni(111) surface partially covered with MnO_x species. Two new features are observed here: a high-frequency shoulder at 2050 cm^{-1} and another at 1620 cm^{-1}. The 2050-cm^{-1} energy loss peak can be attributed to either on top CO or CO adsorbed on a cationic site (*29–31*). A similar feature was observed previously on TiO_x/Ni (*7*). In the first interpretation, with

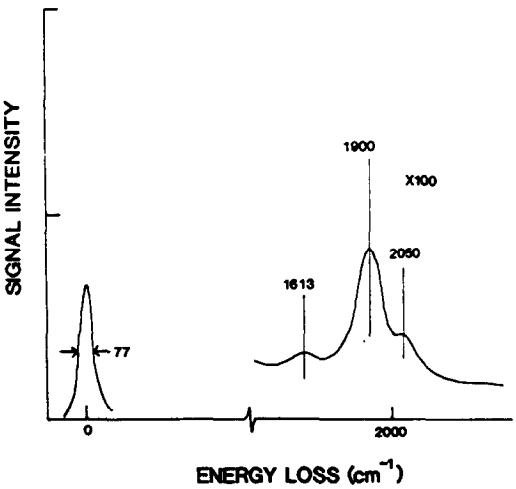

FIG. 6. High-resolution electron energy loss spectrum of 30 L CO adsorbed on a MnO_x-modified Ni(111) surface at 200°K. The Auger Mn (589 eV)/Ni (848 eV) = 0.08.

increased oxide coverage, the concentration of on top sites should increase relative to twofold bridge sites, hence the appearance of the 2050-cm^{-1} feature. In the second interpretation, the specific cationic sites involved are probably not MnO_x alone as complete MnO_x coverage deactivates CO adsorption at 200°K. Most probably, these sites may involve some MnO_x/Ni ensembles. We do not have additional information to favor one interpretation over another at this time.

Ichikawa and co-worker (*27*) observed an anomalously low C–O stretch when a manganese-promoted Rh/SiO_2 catalyst was exposed to CO. The interpretation by Sachtler and co-workers (*26*) is that the CO molecule adsorbed on the Rh surface is activated on the oxygen end by surface Mn, thereby weakening the C–O bond and lowering the C–O stretching frequency. That is, CO is adsorbed near certain Rh–Mn ensembles. A possible interpretation of our present observation is that the 1620-cm^{-1} feature is due to CO adsorbed at or near Ni/MnO_x perimeter sites. A corollary of this interpretation is that the 305°K thermal desorption peak and the 1620-cm^{-1} energy loss peak describe the same adsorbed CO species. Figure 7 shows a series of loss spectra due to CO adsorbed on Ni(111) partially covered with MnO_x. Figure 7a was taken after 30 L CO exposure at 200°K, essentially the same as Fig. 6. Figures 7b, 7c, and 7d were taken at room temperature after the surface had been heated to 325°K for 5, 10, and 15 min respectively. The 1620-cm^{-1} peak disappeared immediately after the surface was heated to 325°K. This observation is fully consistent with our interpretation.

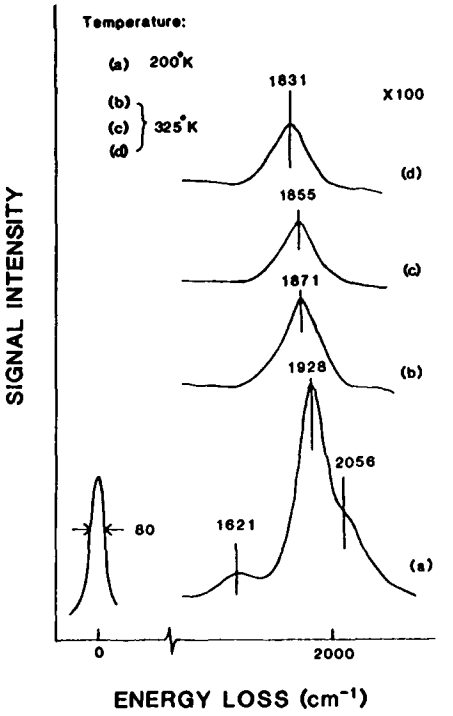

FIG. 7. Series of high-resolution electron energy loss spectra of CO on a MnO_x-modified Ni(111) surface taken under various conditions: (a) 30 L CO at 200°K; (b) after the surface of a has been heated to 325°K for 5 min; (c) after the surface of b has been heated at 325°K for another 5 min; (d) after the surface of c has been heated at 325°K for another 5 min. (Auger Mn (589 eV)/N: (848 eV) = 0.11).

SIGNIFICANCE OF PERIMETER SITES

Changes in chemical activity of a catalyst when it is in the SMSI state have been widely reported. In most cases, enhancement in CO hydrogenation activity is observed, and the studied systems include Ni/TiO_2 (*16, 23*), Rh/TiO_2 (*32*), Pt/TiO_2 (*17, 20*), Pd/TiO_2 (*18, 19*), Pd/La_2O_3 (*33*), $NiFe/TiO_2$ (*34*), and Ni/Nb_2O_5 (*35*). There are also cases in which activities do not change or even decrease when the catalyst is in the SMSI state. Some examples are ethane and *n*-butane hydrogenolysis over Rh/TiO_2 (*4, 36*), Pt/TiO_2 (*36*), Ir/TiO_2 (*36*), and Ni/Nb_2O_5 (*35*) where a suppression in activity is observed. Therefore, the manifestation of SMSI depends on the specific system and the specific reaction involved.

In studying SMSI effects in nickel/titania catalysts, Burch and Flambard (*37*) found that only a fraction of the available metal surface is active to give an enhanced CO hydrogenation activity, and they suggested that these active sites were created at the

oxide–metal interface. Similar observations were reported by Vannice *et al.* in which they found that for Pd/TiO_2 (*18*) and Pt/TiO_2 (*20*) systems in the SMSI state, although there was a higher activity for CO hydrogenation, only a small fraction (0.01 or less) of the surface metal sites constituted active sites for the reaction. Again, they suggested that there are special active sites existing at the metal–titania interface and that these sites could interact with the oxygen end of a CO molecule adsorbed on the metal surface to facilitate its dissociation (*25*). In the present work, weakly bonded CO (305°K thermal desorption peak) is found with a lower C–O stretching frequency (1620-cm^{-1} HREELS peak) which we attributed to CO adsorbed at or near the perimeter sites, with the oxygen end activated by the MnO_x species. The population of these active sites is only a small fraction of the total surface metal sites as inferred from our thermal desorption data. These results are consistent with those we just discussed. One would therefore expect that the CO dissociation process under these conditions would become easier and faster (*26*). Such an enhanced CO dissociation as well as enhanced CO hydrogenation activity were observed recently in Rh/TiO_2 (*27*) and Ni/TiO_2 (*38*). In another study of TiO_x-modified Ni(111) surface (where x was between 1.0 and 1.5), Chung and co-workers found that the methane turnover frequency varies with TiO_x coverage, and that a maximum was achieved at an optimum Ti coverage of about 1.5×10^{14} cm^{-2} (*23*). From this result, one can deduce that neither clean Ni sites nor oxide sites alone could generate this maximum methanation activity. This again is consistent with the present observation and suggests that metal–oxide perimeter sites are likely to be responsible for the observed activity enhancement.

In contrast to the CO hydrogenation reaction, the hydrogenolysis reaction involves the breaking of C–C bonds, which occurs with lower turnover frequency with the induction of SMSI, indicating that the perimeter sites have little or no C–C bond-breaking activity. Therefore, the suppressed reaction activity is simply due to the loss of metal surface sites (*4*).

It is generally accepted that SMSI effects can be generated only when the support oxide is reducible and migrates to the metal surface rapidly under typical SMSI reduction conditions. For SiO_2-supported metals reduced at about 700°K, catalytic properties are mainly unaffected (*17, 32*). Ko *et al.* found that the SMSI effect is less pronounced for $Ni/Nb_2O_5/SiO_2$ than for Ni/Nb_2O_5 (*39*). This suggests that under typical reduction conditions to induce SMSI, either the migration rate of SiO_2 is too low to produce any observable surface concentration or the oxide is so stable that no interaction between the metal and the support takes place.

In studying the chemisorption of a TiO_x-modified Pt surface, Dwyer *et al.* showed a linear relationship between the extent of CO or H_2 chemisorption suppression and the number of Pt sites physically blocked by the oxide (*21*). Takatani and Chung found that the suppression of CO on Ni is not linear with titania coverage (*8*). Similar nonlinear suppression of CO chemisorption on TiO_x-modified Rh surfaces was reported recently by Bell and co-workers (*40*). The present results show that the suppression of CO on Ni is almost linear with MnO_x coverage. Rather than interpreting this difference as due to some fundamental change in the effective range of SMSI, we believe that this is simply due to a difference in oxide morphology.

Recent research has related the enhancement of CO hydrogenation activity to the Ti^{3+} centers located at the periphery of the titania–metal interface. An important fact is that in the presence of H_2O as a by-product of the CO hydrogenation reaction, Ti^{3+} species and SMSI effects are quite durable under the reaction conditions. Dwyer *et al.* found using XPS that Ti^{3+} was clearly evident after 16 h exposure to CO

and H_2 at 5% CO conversion (*41*). Greenlief *et al.* found that Ti^{3+} at the oxide–metal interface cannot be fully oxidized to Ti^{4+} when the oxide was exposed to 10^{-7} Torr of O_2 at 650°K for up to 1 h (*42*), which would ordinarily easily oxidize Ti^{3+}. Therefore, by forming oxide–metal ensembles at the perimeter sites on the surface, the metal atoms somehow stabilize Ti^{3+} in its reduced state against oxidation and make SMSI effects durable under CO–H_2 synthesis conditions.

CONCLUSIONS

1. CO chemisorption has been performed on Ni(111) and MnO_x-modified Ni(111) surfaces at 200°K. From thermal desorption and energy loss spectra, it is found that the presence of surface MnO_x species suppresses CO chemisorption, and the suppression is almost a linear function of oxide coverage.

2. For CO adsorbed on a MnO_x-modified Ni(111) surface, additional features of both a lower temperature thermal desorption peak at 305°K and a lower C–O stretching frequency peak at 1620 cm^{-1} are observed. The 1620-cm^{-1} energy loss peak disappears when the surface is heated to 325°K, which indicates that these two features come from the same new CO adsorption mode.

3. Results from CO thermal desorption and from Monte Carlo simulation of an oxide-modified face-centered-cubic (111) surface show that the 305°K TDS peak intensity and the surface perimeter site population vary with oxide coverage in a similar manner. This suggests that the 305°K TDS peak and the 1620-cm^{-1} energy loss peak are due to the CO adsorption at or near the surface MnO_x/Ni perimeter sites. Such an adsorption state is believed to be important in enhancing the CO hydrogenation activity in an SMSI system.

ACKNOWLEDGMENTS

Acknowledgment is made to the donors of the Petroleum Research Fund, administered by the American Chemical Society, for support of this research. We thank Professor Sachtler and Dr. Ichikawa for many illuminating discussions.

REFERENCES

1. Tauster, S. J., Fung, S. C., and Garten, R. L., *J. Amer. Chem. Soc.* **100,** 170 (1978).
2. Tauster, S. J., and Fung, S. C., *J. Catal.* **55,** 29 (1978).
3. Santos, J., Phillips, J., and Dumesic, J. A., *J. Catal.* **81,** 147 (1983).
4. Eresasco, D., and Haller, G. L., *J. Catal.* **82,** 279 (1983).
5. Jiang, X. Z., Hayden, T. F., and Dumesic, J. A., *J. Catal.* **83,** 168 (1983).
6. Hicks, R. F., Yen, Q. J., and Bell, A. T., *J. Catal.* **89,** 498 (1984).
7. Takatani, S., and Chung, Y. W., *J. Catal.* **90,** 75 (1984).
8. Takatani, S., and Chung, Y. W., *Appl. Surf. Sci.* **19,** 341 (1984).
9. Spencer, M. S., *J. Catal.* **93,** 216 (1985).
10. Chung, Y. W., and Zhao, Y. B., *in* "Strong Metal–Support Interactions," ACS Symposium Series 298, p. 54. Amer. Chem. Soc., Washington, DC.
11. Ko, C. S., and Gorte, R. J., *J. Catal.* **90,** 59 (1984).
12. Demmin, R. A., Ko, C. S., and Gorte, R. J., *in* "Strong Metal–Support Interactions," ACS Symposium Series 298, p. 48. Amer. Chem. Soc., Washington, DC.
13. Belton, D. N., Sun, Y.-M., and White, J. M., *J. Phys. Chem.* **88,** 1690 (1984).
14. Belton, D. N., Sun, Y.-M., and White, J. M., *J. Phys. Chem.* **88,** 5172 (1984).
15. Sun, Y.-M., Belton, D. N., and White, J. M., *J. Phys. Chem.* **90,** 5178 (1986).
16. Vannice, M. A., and Garten, R. L., *J. Catal.* **56,** 29 (1979).
17. Vannice, M. A., Twu, C. C., and Moon, S. H., *J. Catal.* **79,** 70 (1983).
18. Vannice, M. A., Wang, S. Y., and Moon, S. H., *J. Catal.* **71,** 152 (1981).
19. Wang, S. Y., Moon, S. H., and Vannice, M. A., *J. Catal.* **71,** 167 (1981).
20. Vannice, M. A., and Twu, C. C., *J. Catal.* **82,** 213 (1983).
21. Dwyer, D. J., Cameron, S. D., and Gland, *J. Surf. Sci.* **195,** 430 (1985).
22. Kao, C. C., Tsai, S. C., and Chung, Y. W., *J. Catal.* **73,** 136 (1982).
23. Chung, Y. W., Xiong, G. X., and Kao, C. C., *J. Catal.* **85,** 237 (1984).
24. Burch, R., and Flambard, A. R., *J. Catal.* **78,** 389 (1982).
25. Vannice, M. A., and Sudhakar, C., *J. Phys. Chem.* **88,** 2429 (1984).
26. Sachtler, W. M. H., Shriver, D. F., Hollenberg, W. B., and Lang, A. F., *J. Catal.* **92,** 429 (1985).

27. Ichikawa, M., and Fukushima, T., *J. Phys. Chem.* **89,** 1564 (1985).
28. Zhao, Y. B., and Chung, Y. W., unpublished results.
29. Erley, W., Ibach, H., Lehwald, S., and Wagner, H., *Surf. Sci.* **83,** 585 (1979).
30. Campuzano, J. C., and Greenler, R. G., *Surf. Sci.* **83,** 301 (1979).
31. Erley, W., Wagner, H., and Ibach, H., *Surf. Sci.* **80,** 612 (1979).
32. Erdohelyi, A., and Solymosi, F., *J. Catal.* **84,** 446 (1983).
33. Hicks, R. F., and Bell, A. T., *J. Catal.* **90,** 205 (1984).
34. Jiang, X. Z., Stevenson, S. A., and Dumesic, J. A., *J. Catal.* **91,** 11 (1985).
35. Ko, E. I., Hupp, J. M., and Wagner, N. J., *J. Catal.* **86,** 315 (1984).
36. Meriaudeau, P., Ellestad, O. H., Dufaux, M., and Naccache, C., *J. Catal.* **75,** 243 (1982).
37. Burch, R., and Flambard, R., *J. Catal.* **78,** 389 (1982).
38. Bartholomew, C. H., and Vance, C. K., *J. Catal.* **91,** 78 (1985).
39. Ko, E. I., Bafrali, R., Nuhfer, N. T., and Wagner, N. J., *J. Catal.* **95,** 260 (1985).
40. Levin, M., Salmeron, M., Bell, A. T., and Somorjai, G. A., *Surf. Sci.* **169,** 123 (1986).
41. Dwyer, D. J., Robbins, J. L., Cameron, S. D., Dudash, N., and Hardenbegh, J., *in* "Strong Metal–Support Interactions," ACS Symposium Series 298, p. 21. Amer. Chem. Soc., Washington, DC.
42. Greenlief, C. M., White, J. M., Ko, C. S., and Gorte, R. J., *J. Phys. Chem.* **89,** 5025 (1985).